XVIII International Conference on Water Resources
CMWR 2010
J. Carrera (Ed)
CIMNE, Barcelona 2010

PARTIALLY SATURATED OSCILLATORY FLOW IN A SANDY BEACH (NUMERICAL MODELING)

Khalil ALASTAL, Rachid ABABOU and Dominique ASTRUC

Institut de Mécanique des Fluides de Toulouse (IMFT),
Allée du Professeur Camille Soula, 31400 Toulouse, France.
Email addresses: alastal@imft.fr, ababou@imft.fr, astruc@imft.fr.

Key words: Porous media, numerical modeling, partially saturated flow, Richards equation, free surface oscillations, sorptivity.

Summary. In this paper, numerical modeling of oscillatory flow in 1D porous column is developed, validated and interpreted in terms of space-time scales in order to assist in the design and interpretation of 1D and 2D laboratory experiment.

1 INTRODUCTION

Surface/subsurface flow interactions concern a wide range of applications, from beach morphodynamics (swash zone), to harbor engineering and hydrology (e.g., man-made structures such as porous dykes and earth dams).

In the context of beach dynamics, two types of periodic 'forcing' will be considered:

1. low frequency / long tidal waves (approximated as quasi-static reservoir oscillations);
2. high frequency / short waves (complex nonlinear surface wave dynamics, including: overspill, run up/run down processes, and erosion near the swash zone).

In this paper, oscillatory flow in the presence of a sandy beach is studied numerically using Richards's equation for unsaturated or partially saturated flow, with oscillatory pressure-based boundary conditions. With this in mind, the numerical simulations and analyses are currently being conducted as follows:

- Validation test for the numerical procedure through 1D infiltration problem.
- Analyses of sudden recharge and drainage on a 1D porous column.
- Analyses of forced oscillations in a partially saturated 1D column, and interpretation in terms of space-time scales. This will help in defining the appropriate scales for a more complex 2D slab experiment.

2 NUMERICAL MODELING USING BIGFLOW

The 3D finite volume flow code 'BIGFLOW' has been widely described, documented, tested and benchmarked[1,2,3]. The equational model of BIGFLOW is a generalized Darcy-type equation, with a mixed formulation of mass conservation, capable of simulating various types of flows within the same domain. It is of the form:

$$\begin{cases} \dfrac{\partial \theta(h,\vec{x})}{\partial t} = -\vec{\nabla} \bullet \vec{q} \\ \vec{q} = -\vec{\vec{K}}\left(h, \vec{\nabla} H, \vec{x}\right)\vec{\nabla} H \\ H = h + \vec{g}(\vec{x}) \bullet \vec{x} \end{cases} \tag{1}$$

where only the first equation is actually solved (after insertion of the second and third equations). The first equation expresses mass conservation with a known water retention curve $\theta(h)$; the second equation is a generalized nonlinear flux-gradient law with tensorial hydraulic conductivity/transmissivity (K); and the third equation is the relation between total head (H) and pressure head or water depth (h) via a normalized gravitational vector (g).

3 SOIL PARAMETERS & CHARACTERISTIC SPACE-TIME SCALES

In the case of 3D flow in partially saturated/unsaturated media, 'h' is the pressure head relative to atmospheric pressure [L], $K(h)$ is the unsaturated conductivity [LT^{-1}], and $\theta(h)$ is volumetric water content [L^3/L^3]. Two main functional models were considered in BIGFLOW 3D for the nonlinear curves: *Van Genuchten / Mualem (VGM)* and *Exponential (EXP)*. In this paper, VGM model is used. Other important relations can be derived from these properties such as[4]: moisture capacity $C(h)$; hydraulic diffusivity $D(h)$; gravitational speed $U(h)$; and capillary dispersion length $\lambda(h)$. The global capillary length scale of the soil can be defined via the point of maximum moisture capacity, i.e., the inflexion point of $\theta(h)$, which leads to[4]:

$$\lambda_{CAP} = \frac{1}{\alpha}\left(1 - \frac{1}{n}\right)^{1/n} \tag{2}$$

where "α" is the Van Genuchten pressure scaling parameter (inverse length units), and "n" is the Van Genuchten/Mualem exponent (dimensionless positive real number). The λ_{CAP} values obtained for the 3 soils considered in this work can be found in the Table 1 below. Finally, note that several characteristic time scales can be formed (gravitational, capillary,…): we use only one of them here, the time scale "t_{GRAV}", as explained immediately below (infiltration tests).

4 VALIDATION TESTS WITH CONTINUOUS UNSATURATED INFILTRATION

In this section, 1D continuous infiltration through a deep homogeneous soil is used to validate the numerical procedure, using the Van Genuchten/Mualem model in BIGFLOW 3D. The numerical results are compared with those of Philip's series solution, which was programmed in Matlab after the method of Vauclin et al.[5]. Permeability and sorptivity are identified from the numerical cumulative infiltration rate via an optimal fit procedure, and compared to the actual permeability and sorptivity (the latter is deduced from other parameters through Parlange's expression).

4.1 Theoretical background

Over the past years, numerous analytical and semi-empirical equations for 1D infiltration have been developed[6]. Philip[7] has shown that a nonlinear solution can be obtained by a time expansion procedure in the case of a constant water content imposed at the surface. He derived the following series solution for the cumulative infiltration $I(t)$ [L] :

$$I(t) = St^{1/2} + (A_2 + K_0)t + A_3 t^{3/2} + A_4 t^2 + \cdots \tag{3}$$

where K_0 is the initial hydraulic conductivity [$L.T^{-1}$], t is time [T] , S is the sorptivity [$L.T^{-1/2}$]. The sorptivity 'S' and the A's depend on the initial (θ_0) and boundary (θ_1) conditions. Sorptivity characterizes the ability of the soil to absorb water by capillary diffusion (in the absence of gravity). In practice, it is sufficient to use the two-parameter equation of the form:

$$I(t) = St^{1/2} + At \tag{4}$$

One of the problems involved in Philip's solution is that the time series solution becomes divergent for large times no matter how many terms are developed. Thus the above solution is only valid for a limited time range. The time limit is mostly set at t_{GRAV} (a time for which the gravity forces are supposed to become predominant over the capillary forces):

$$t_{GRAV} = \left(\frac{S(\theta_1, \theta_0,)}{K_1 - K_0}\right)^2 \tag{5}$$

A different solution was proposed by Parlange[8] resulting in the following sorptivity expression:

$$S^2 = \int_{\theta_0}^{\theta_1} [\theta_1 + \theta - 2\theta_0] D(\theta) d\theta \tag{6}$$

where D is moisture diffusivity $D = K/C = K\, dh/d\theta$ [$L^2.T^{-1}$].

4.2 Validation test

A 1D column with the initial and boundary conditions shown in figure 1 is used for simulating the 1D infiltration problem in BIGFLOW code. Table 1 shows the hydraulic characteristics of the porous media used in the simulation.

Parameters		Soil No.1 Fine Sand	Soil No.2 Medium Sand	Soil No.3 Loam
K_{sat} (m/s)		2.7×10^{-4}	2.0×10^{-4}	3.66×10^{-6}
θ_{sat}		0.411	0.35	0.52
θ_{dry}		0.0073	0.0147	0.218
VGM model parameters	α (m^{-1})	5.85	11.47	1.15
	$1/\alpha$ (cm)	17.08	8.71	86.95
	λ_{CAP} (cm)	15.34	6.11	62.25
	n	3.32	1.98	2.03

Table 1: Hydraulic characteristics of porous media.

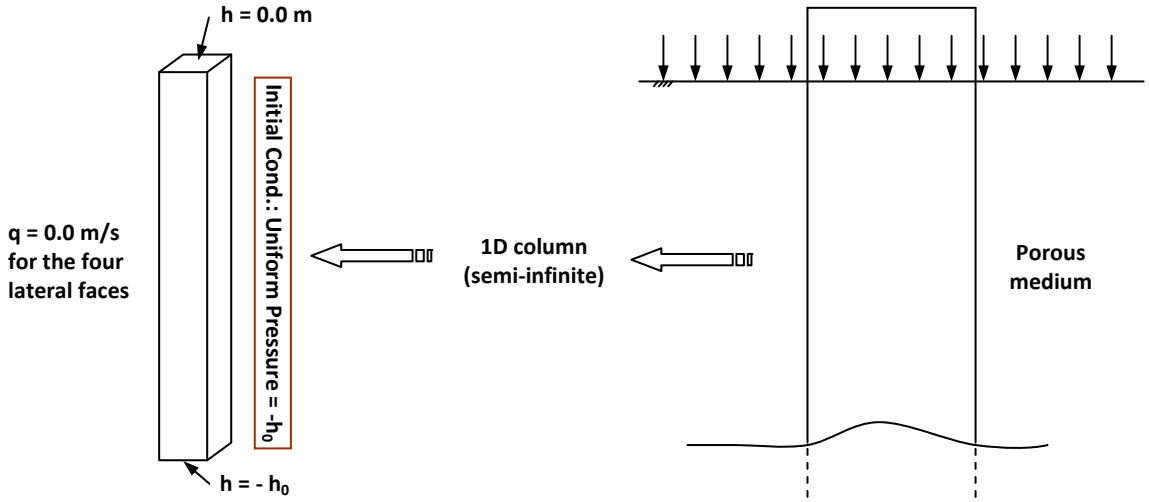

Figure 1: Initial and boundary conditions used in the infiltration test for the 3 soils.

4.3 Results and analysis

Simulation results of the infiltration test for soil No.1 (fine sand) are presented in figure 2. The y-intercept and the slope of $I/\sqrt{t}$ versus$\sqrt{t}$ curve give the *S* and *A* values (see equation 4). The maximum time of BIGFLOW simulation is about t_{GRAV}. A summary of the results for the three soils is given in Table 2.

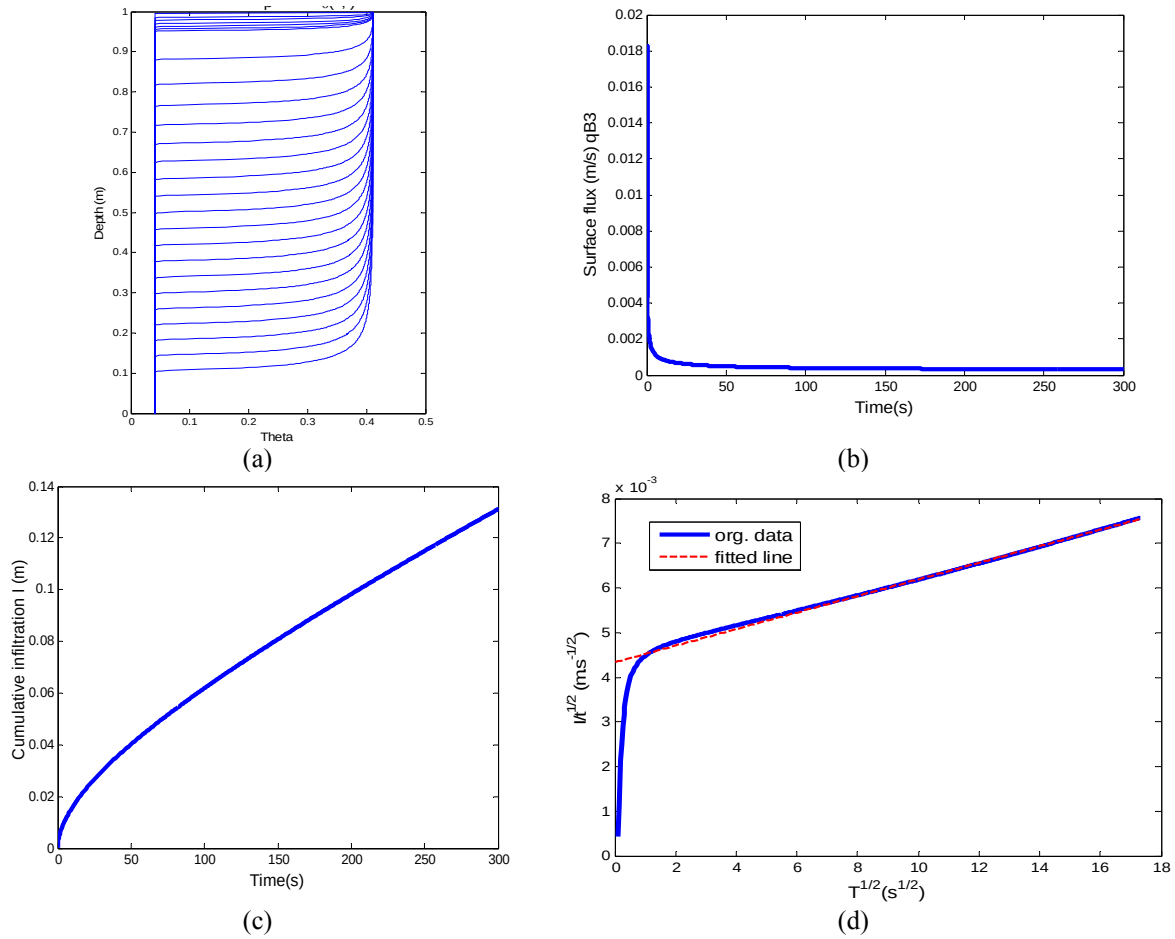

Figure 2: Bigflow results of the infiltration problem. (a) evolution of moisture profiles θ(z,t), (b) surface flux versus time, (c) Cumulative infiltration versus time, (d) $I/\sqrt{t}$ versus $\sqrt{t}$ including the fitting parameters.

Infiltration Parameters	**Soil No.1 Fine Sand**	**Soil No.2 Medium Sand**	**Soil No.3 Loam**
A (m/s)	1.686×10^{-4}	1.121×10^{-3}	1.762×10^{-6}
A/K_{sat} (%)	62.4	56.05	48.14
S, Sorptivity (m/$s^{1/2}$) BIGFLOW	4.48×10^{-3}	1.815×10^{-3}	8.712×10^{-4}
S, Sorptivity (m/$s^{1/2}$) Parlange	4.57×10^{-3}	1.908×10^{-3}	8.682×10^{-4}
S, Sorptivity (m/$s^{1/2}$) Philip/Vauclin	4.15×10^{-3}	1.898×10^{-3}	8.498×10^{-4}
t_{grav}, average (sec)	266	88	55643

Table 2: Infiltration parameters' results obtained from different methods.

By comparing the simulation results with those of Philip's and Parlange solutions, a good agreement is found in terms of sorptivity values. Note that the simulation results were analysed through an optimal fit procedure, providing that a very short initial phase of the simulated infiltration is removed (indeed the initial flux in this experiment is infinite in theory).

The results also show that for all cases: $1/3 < A/K_{SAT} < 2/3$ as mentioned in the literature[9].

5 NUMERICAL EXPERIMENTS & ANALYSES – UNSATURATED DYNAMICS

Numerical simulations are conducted with the BIGFLOW 3D code in a partially saturated 1D porous column under highly "dynamic" conditions. The following cases are studied: **(1)** sudden recharge and drainage processes; **(2)** forced periodic oscillations. In what follows, we present only the results for soil N°3 (Loam). In all simulations, suitable numerical parameters were chosen to obtain good numerical results in terms of mass balance (net boundary flux versus mass flux), and convergence of both nonlinear solver (Incremental Picard) and matrix solver (Preconditioned Conjugate Gradients with Diagonal Scaling).

5.1 Sudden recharge and sudden drainage:

A hydrostatic pressure is applied as an initial condition, with the free surface located at z = 0.5m (z is elevation from the bottom). A sudden recharge process is obtained by applying a constant pressure boundary condition at the bottom of the column (z = 0), with positive pressure "h_{BC}" greater than the initial hydrostatic pressure ($h_{BC} = h_{IN} + 0.10$ m). The resulting free surface at infinite time (steady state) should be located at z = 0.5 + 0.1 = 0.6 m. On the other hand, another numerical experiment is also conducted, this time for sudden drainage process. A bottom pressure condition is applied such that $h_{BC} = h_{IN} - 0.10$ m. The resulting free surface in the column should then descend from z = 0.5m initially to z = 0.5 - 0.1 = 0.4 m at infinite time (steady state). The maximum time of simulation is chosen to be $t_{MAX} = 10^5$sec ($t_{MAX} \approx 2t_{GRAV} \approx 1$day). Figure 3 shows the free surface position versus time for the two cases.

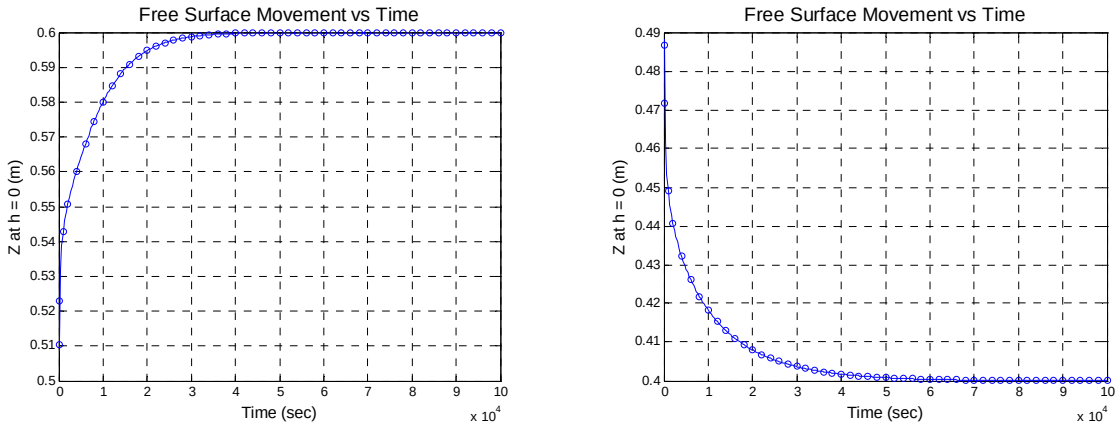

(a) (b)

Figure 3: Free surface position versus time for (a) sudden recharge, (b) sudden drainage.

The benefit of the above recharge and drainage simulations is that they provide information on the response time scale of the partially saturated soil column. This response time can then be used for selecting the appropriate periods for the case of periodic forcing, i.e., short waves

and long tidal waves, idealized by a periodic pressure condition applied at the bottom of the column.

Thus, in the case of forced oscillations, if the applied pressure wave has a quarter-period $T_p/4 = 0.5 \times 10^4$ sec and an amplitude of 0.10 m, then referring to the above recharge/drainage simulations, it is expected that this periodic wave will generate a free surface wave of about 0.06m amplitude (less than the amplitude 0.10m of the applied wave). Therefore this period corresponds to a "high frequency/short wave" type at least in terms of the hydrodynamic response of this soil. On the other hand, if the quarter-period of the applied pressure wave is larger, say $T_p/4 = 6 \times 10^4$ sec, with the same amplitude, then we expect that the free surface will oscillate with nearly the same amplitude and phase as the applied bottom pressure wave. This period corresponds to a "low frequency / long wave" type, in terms of soil response. See the ensuing discussion in the next section.

5.2 Forced oscillations:

To study the effect of forced oscillations, a sinusoidal pressure wave of the form $h(t) = h_0 + A \sin(\omega t)$ is imposed at the bottom face of the porous column; where: h_0 is the average pressure head of the wave, chosen to coincide with the initial hydrostatic level (0.5m); "A" is the amplitude of the pressure wave (A = 0.1m, same as the head variation imposed in the sudden recharge/drainage problems); $\omega = 2\pi/T_P$ is the angular frequency; and T_P is the period of the wave. As suggested previously, two different wave periods are chosen, the "short wave" period T_{P1} = 20 000sec, and the "long wave" period T_{P2} = 240 000sec. Figures 4 and 5 show the results of simulations for periods T_{P1} and T_{P2}, respectively. Note that the ratio A/h_o is less than 1, so the oscillatory bottom pressure remains always positive ($\forall t$).

The simulation results confirm our expectations as stated previously. For the "short wave" (T_{P1}), the oscillations of the free surface height Z(t) do not follow the pressure wave applied at the bottom. The amplitude of the free surface is 0.055m, only slightly less than the value 0.06m obtained for the sudden recharge case, This slight discrepancy between the two cases (periodic/sudden) is not unsurprising given the gradual versus abrupt changes imposed at the bottom boundary (compare the two cases at time $t = T_{P1}/4$ = 5000sec).

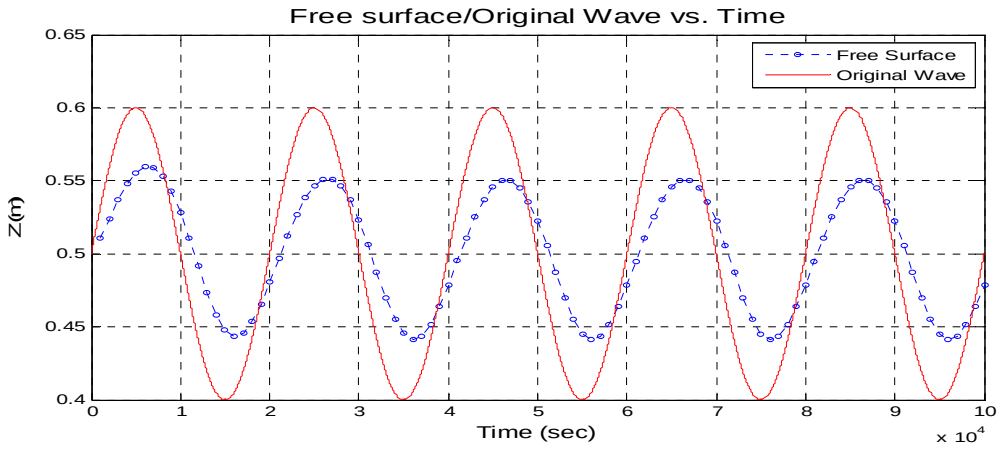

Figure 4: Comparison between free surface position (dotted line) and the applied pressure wave (solid line) versus time for the "short" period, T_{P1} = 20 000 sec ≈ t_{GRAV} / 3 (Loam soil N°3).

On the other hand, for the "long wave" (T_{P2}), the oscillations of the free surface height Z(t) are almost identical with those of the bottom pressure (indistinguishable with respect to the amplitude, but still slightly distinct in terms of phase lag). In total, these results confirm that the two chosen periods, short and long, have very different effects in terms of the response of the unsaturated soil column (free surface height movements Z(t)).

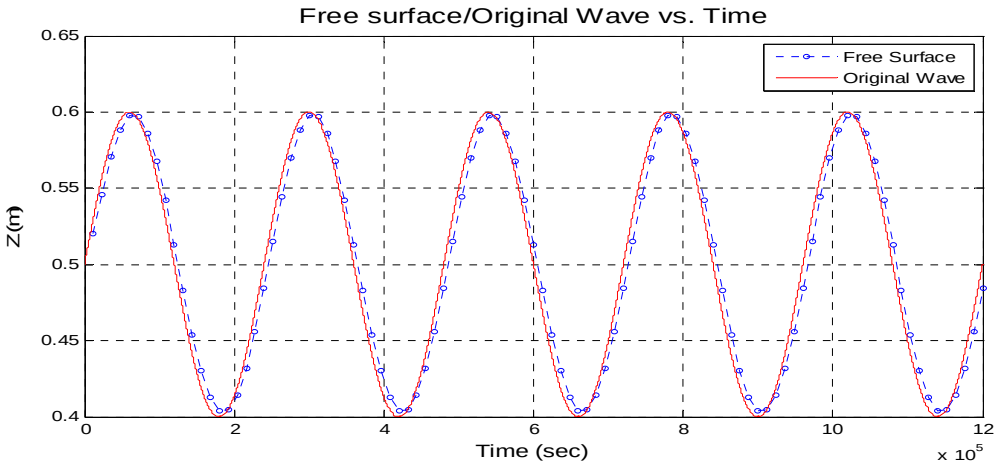

Figure 5: Comparison between free surface position (dotted line) and the applied pressure wave (solid line) versus time for the "short" period, T_{P2} = 240 000 sec ≈ $4t_{GRAV}$ (Loam soil N°3).

The next step is to study the effects of the period (T_P) and the average height (h_0) of the applied bottom pressure wave, on the phase lag (*delay*) between this input wave and the free surface wave Z(t). For this purpose, two sets of numerical simulations were conducted with a range of T_P and h_0 values. **Figure 6** shows the final result of these simulations. First, from figure 6(a), it is clear that the phase lag (*in radians*) between the two waves decreases as the wave period T_P increases. Indeed, this is because; by increasing T_P, more time is given for the free surface to follow the applied wave and therefore, a lower phase difference is obtained. Secondly, from figure 6(b), we can deduce that as the average pressure wave height (h_0) applied at the bottom increases, the phase lag increases also. This may be due to several effects which are currently being analyzed (note that the column has finite height and a zero flux condition is imposed on top).

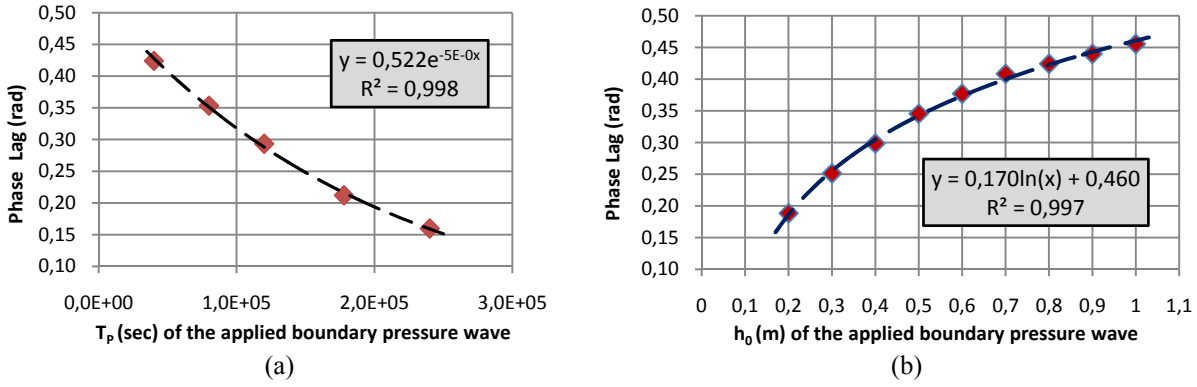

Figure 6: Phase lag plotted versus (a) pressure wave period T_P, and (b) average pressure wave height h_0. The ordinate is the phase lag between the boundary pressure and the resulting free surface wave (Loam soil N°3).

Further investigations are done to study the effect of the amplitude (of the applied pressure wave at the bottom boundary (*A*)) on the free surface evolution. Figure 7(a) shows that as the amplitude [*nominalised by* h_0] increases, the phase lag between the two waves decreases. It is also noted from figure 7(b) that as the amplitude of the applied boundary pressure wave approaching the average wave height, the resulting free surface is no longer symmetric; this is because the effect of the bottom boundary condition becomes dominant.

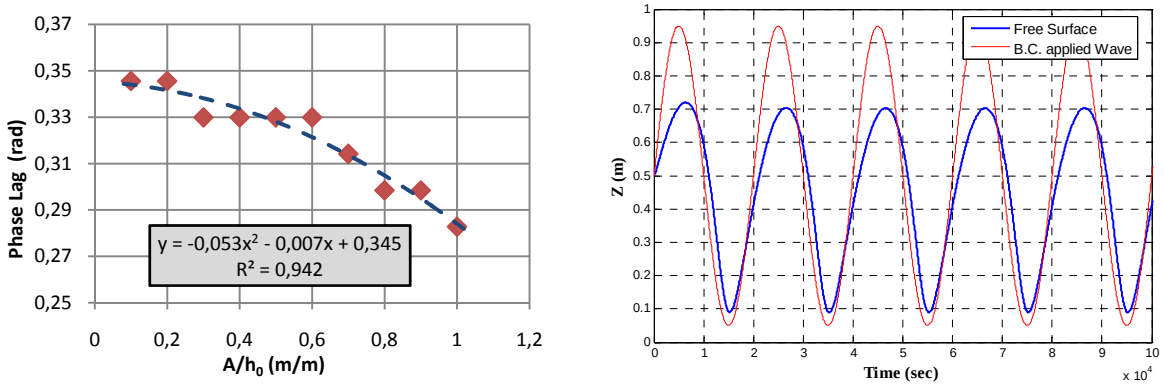

(a) (b)

Figure 7: (a) The effect of the amplitude A on the phase lag between the applied boundary pressure wave and the resulting free surface wave. (b) The evolution of the resulting free surface compared to that of the pressure wave applied at the bottom boundary for $A/h_0 = 0.9$ (Loam soil N°3).

6 "EULERIAN" PRESSURE ANALYSIS (POINT TO POINT ANALYSIS):

In this part, instead of analysing the free surface evolution (as in the previous section), we are interested in interpreting the results focusing on pressure evolution h(z,t) at a specific level "z" as a result of an applied pressure wave h(0,t) at the bottom boundary. In what follows, we present the results for a new fine sand ($K_{SAT}=1.5\times10^{-4}$, $\theta_{SAT} = 0.38$, VGM parameters: $\alpha = 4.6\ m^{-1}$, $n = 5$).

Figure 8 shows the pressure evolution at four different points along the column [(a) h(0,t), (b) h(0.5,t), (c) h(0.7,t) and (d) h(0.85,t)] as a result of an oscillatory pressure boundary condition [$h(0,t) = 0.5 + 0.1 \sin(wt)$]. These figures clearly show the damping effect on the applied pressure wave through the length of column. Moreover, it is observed that the effect of the bottom boundary pressure wave disappears at height $z = 1.1m$ from the bottom of the column (at $z = 1.1m$ ➔ $h = -0.6m$ for all $t \leq t_{MAX\ SIMULATION}$).

Additionally, by analysing the phase lag along the column in the fully saturated zone (from z=0 to z=0.4m) and in the variably saturated zone (between z=0.4 and z=0.6m), we can deduce from figure 9(a) that by moving further away from the bottom boundary, the phase lag increases superlinearly (up to a point). This may be due to several effects combining darcian friction losses and unsaturated capillary zone dynamics. This particular behaviour is not completely elucidated at this time, and requires further investigation.

On the other hand, figure 9(b) shows that as the average height (h_0) of the applied pressure wave increases, the phase lag between this boundary pressure wave and the pressure obtained at a height $z=h_0$ increases also. This result confirms what was previously obtained in Section 5 for the phase lag between the bottom pressure and the resulting free surface height.

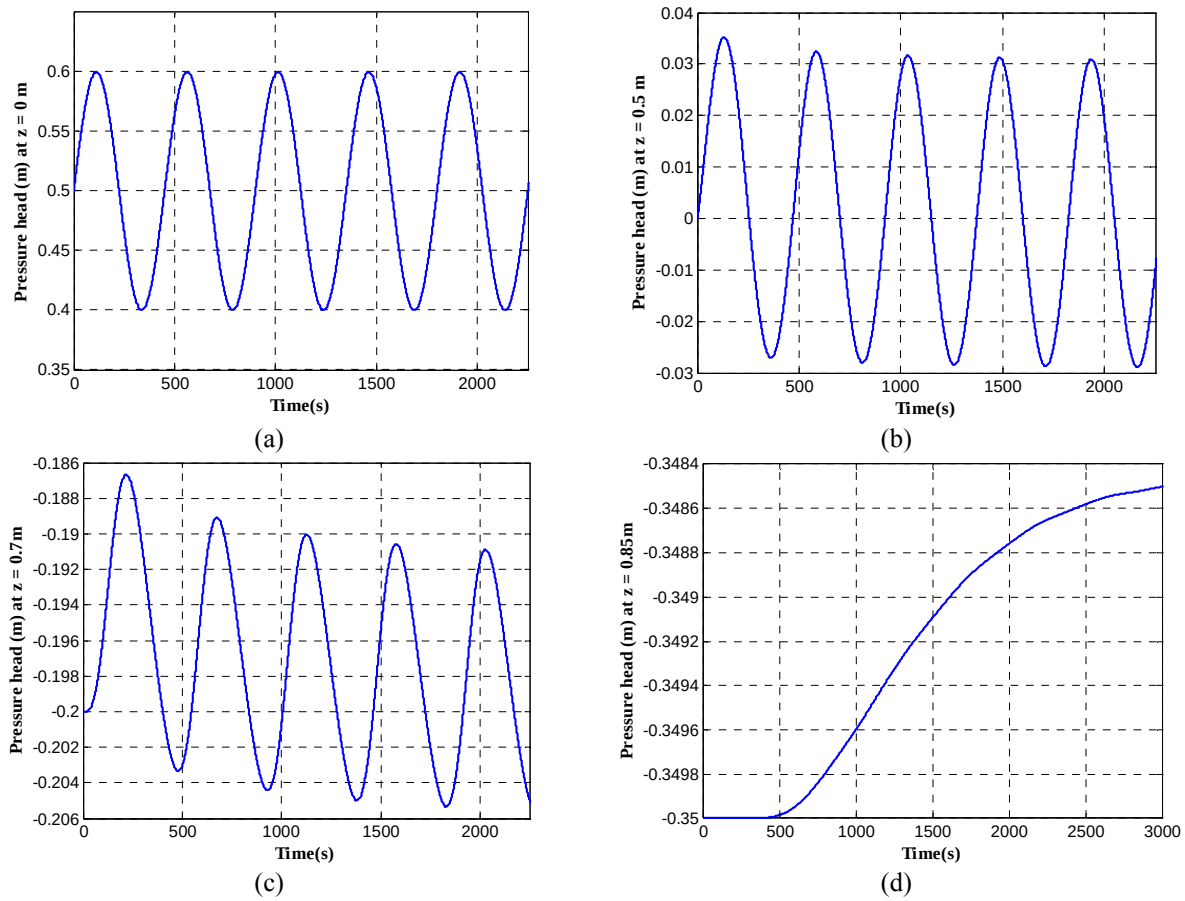

Figure 8: Pressure evolution along the fine sand column at (a) the bottom boundary z =0m, (b) z = 0.5m, (c) z= 0.7m, (d) z = 0.85m. The parameters of the applied bottom boundary pressure wave are: A = 0.1m, h_0 = 0.5m, Tp = 450sec.

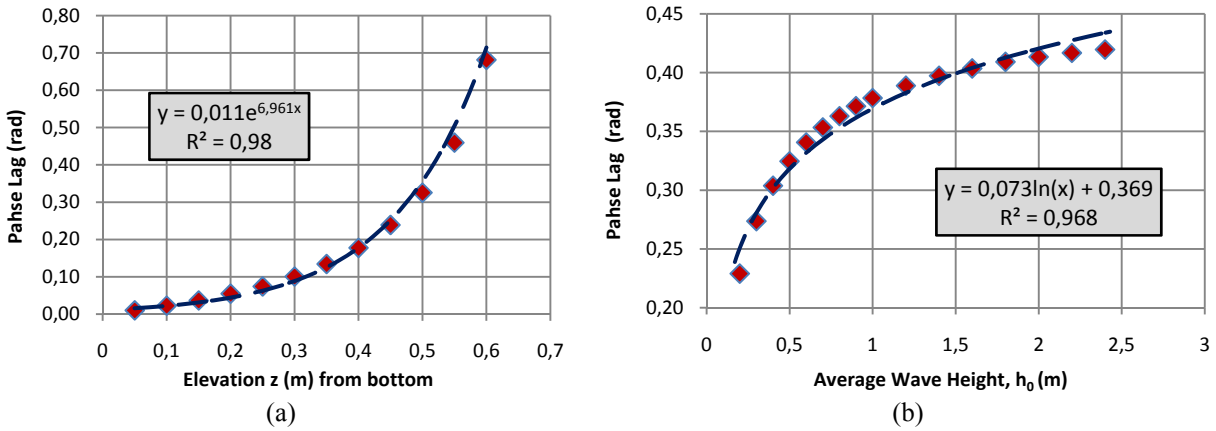

Figure 9: (a) Phase lag evolution along the fine sand column (vertical profile) for wave parameters A = 0.1m, h_0 = 0.5m, Tp = 450sec. (b) Phase lag versus average pressure wave height h_0 for wave parameters A = 0.1m, h_0 = variable, Tp = 450sec (this is the phase lag between boundary pressure and the resulting pressure at height z = h_0).

7 CONCLUSIONS

In this paper, a set of numerical modeling was conducted to study the effect of vertical oscillatory flow in a 1D partially saturated porous column. Through these simulations, two wave types can be distinguished (low frequency waves / high frequency waves) by an appropriate comparison with the characteristic time scale of the soil.

Furthermore, the resulting oscillations of the free surface height Z(t) were analyzed and the simulations illustrate the effect of wave frequency on phase delay. In addition to that, the pressure evolution and the phase lag along the column are also analysed.

The results of these numerical experiments will assist in the design and interpretation of laboratory experiments, including a 1D partially saturated column experiment, as well as a more complex 2D slab experiment.

REFERENCES

[1] Ababou R. and A.C. Bagtzoglou, *BIGFLOW: A numerical code for simulating flow in variably saturated, heterogeneous geologic media (Theory and user's manual, version 1.1)*". Report NUREG/CR-6028, U.S. Nuclear Regulatory Commission, Government Printing Office, Washington D.C., U.S.A., 139 pp., (1993).

[2] Ababou R. and A. Al-Bitar, *Coupled Surface / Subsurface Flow Systems : Numerical Modeling.* Chap. 7 in "Overexploitation & Contamination of Shared Groundwater Resources". NATO-ASI: Adv. Stud. Instit. Series, C.J.G. Darnault (ed.), Springer Science & Business Media BV, pp. 105-117, (2008).

[3] Bailly D., R. Ababou and M. Quintard , *Geometric Characterization, Hydraulic Behavior and Upscaling of Fissured Geologic Media*. Journal of Mathematics and Computers in Simulation, Special Issue MAMERN 2007, 79 3385–3396. Elsevier B.V, (2009).

[4] Ababou R., *Approaches to Large Scale Unsaturated Flow in Heterogeneous, Stratified, and Fractured Geologic Media*. Report NUREG/CR-5743, U.S. Nuclear Regulatory Commission, Government Printing Office, Washington DC, 150 pp., (1991).

[5] Vauclin M., R. Haverkamp and G. Vachaud, *Résolution numérique d'une équation de diffusion non linéaire. Application à l'infiltration de l'eau dans les sols non saturés*. Presses Universitaires de Grenoble, France, (1979).

[6] Espinoza R.D., *Infiltration*, Chap. 6 in "The Handbook of Groundwater Engineering", edited by Jacques Delleur, CRC Press LLC, (1999).

[7] Philip J.R., *The theory of infiltration*. Adv. Hydrosci. 5: 215-305, (1969).

[8] Parlange J.-Y., *On solving the flow equation in unsaturated soils by optimization: Horizontal infiltration*. Soil Sci. Soc. Am. Proc. 39: 415-418, (1975).

[9] Haverkamp R., F. Bouraoui, C. Zammit, and R. Angulo-Jaramillo, *Soil Properties and Moisture Movement in the Unsaturated Zone*, Chap. 5 in "The Handbook of Groundwater Engineering", edited by Jacques Delleur, CRC Press LLC, (1999).